IEEE Access
Multidisciplinary | Rapid Review | Open Access Journal

Received October 29, 2018, accepted November 12, 2018, date of publication November 22, 2018,
date of current version December 27, 2018.

Digital Object Identifier 10.1109/ACCESS.2018.2882914

A Miniaturized Gain-Enhanced Antipodal Vivaldi Antenna and Its Array for 5G Communication Applications

HAIWEN LIU[1], (Senior Member, IEEE), WENJUAN YANG[1], ANXUE ZHANG[1], SHUANGSHUANG ZHU[1], (Student Member, IEEE), ZHENGBIAO WANG[2], (Student Member, IEEE), AND TAOTAO HUANG[1]

[1]School of Electronics and Information Engineering, Xi'an Jiaotong University, Xi'an 710049, China
[2]School of Information Engineering, East China Jiaotong University, Nanchang 330013, China

Corresponding author: Haiwen Liu (haiwen_liu@ hotmail.com)

This work was supported in part by the National Natural Science Foundation of China under Grant U1831201 and Grant 61728106, in part by the Natural Science Foundation of Jiangxi Province of China under Grant 2017ACB20019, and in part by the Science Technology Project and Research Program of Jiangxi Province of China under Grant 2016BCB18010, Grant 20171BBE50056, and Grant 20181BCB24010.

ABSTRACT In this paper, a miniaturized gain-enhanced antipodal Vivaldi antenna (AVA) with gradual corrugated edges (GCEs) and triangular metal directors (MDs) is investigated. Its operating frequency band is extended and the gain is improved at lower frequencies due to the use of GCEs. In addition, the E-plane beam tilt has been removed and the improvements on side-lobe level are achieved. By applying triangular MDs on the two surfaces of the radiation aperture of the AVA, its gain at higher frequencies is improved. Therefore, the gain variation tends to be flat within the whole operating band. Furthermore, a compact 1×8 E-plane AVA array with a small size of $54.4 \times 28.2 \times 0.508$ mm^3 is also designed, fabricated, and measured. A measured gain is 12.3–12.9 dB in the operating frequency band of 24.75–27.5 GHz, which covers the candidate band for the fifth generation (5G) communication. Good directivity, symmetrical radiation patterns, and compact structure make the proposed AVA array suitable for integration in devices for 5G communication applications.

INDEX TERMS Antipodal Vivaldi antenna, gradual corrugated edge, metal director, array, high-gain, 5G.

I. INTRODUCTION

Nowadays, with the rapid advancement and development of millimeter wave (mmWave) technology and the fifth generation (5G) mobile communication networks, the higher frequency band due to the growing need for wider bandwidths and higher data rates are required. Compared with the cellular networks used today (operating at the frequencies less than 4 GHz), 5G mobile networks will use broader mmWave frequency band [1]. So far, Ministry of Industry and Information Technology (MIIT) has prepared the following four frequency bands for 5G technology research and development: 3.3-3.6 GHz, 4.8-5.0 GHz, 24.75-27.5 GHz, and 37-42.5 GHz. In order to meet the needs of the next generation mobile communication system, Vivaldi antenna is a promising candidate for reasons such as planar structure, low cost, easy fabrication and easy integration [2]. Vivaldi antenna was first introduced by Gibson in 1979 [3]. Then, to get wider bandwidth and simplify feeding structure, Gazit proposed an antipodal Vivaldi antenna (AVA) in 1988 [4]. But, AVA needs large size to achieve good radiation performance. With the aim to miniaturize AVA and maintain its good performance, a variety of techniques including comb-shaped slits [5], elliptical corrugations [6], exponential slot edge [7], sine-shaped corrugation [8], rectangular slits at sun-shaped configuration [9] and periodic slit edge [10] are introduced. However, the mentioned AVAs have low gain especially at higher frequencies. So, there is a new challenge to optimize the mmWave AVA design with a relatively small size and high gain.

To increase the gain at higher frequencies, an effective approach is to load a "director" in the aperture of the AVA, which can focus the energy in the end-fire direction. A parasitic elliptical patch and an exponential dielectric lens in the aperture of the AVA are presented in [11] and [12],

respectively, but these two AVAs are lengthened to aperture direction and the overall sizes are increased. Besides, the metamaterials have been used to realize high-gain Vivaldi antenna. In [13], multiple layers anisotropic zero-index metamaterials (ZIM) are integrated with the Vivaldi antenna to obtain high directivity and high gain. In [14], an ultra-wideband metamaterial slab covered AVA with high-gain is presented. The metamaterial slab sucks energy from the tapered slot and the flare termination of the AVA and transmits the energy to the end-fire direction. However, the size and complexity of these designs increase by loading metamaterials.

Recently, to satisfy the demands of high radiation efficiency, high gain and stable radiation pattern of the 5G mobile communication applications, Vivaldi antenna arrays have been developed. A linear phased array of eight tapered slot antenna (TSA) in the top portion of the mobile-phone PCB and a 64-elemetns TSA array for 5G channel measurement applications are designed in [15]. Due to the advantages of the substrate integrated waveguide (SIW) technology especially in mmWave frequency band, an AVA array based on SIW is investigated for operating band at 42 GHz in [16]. A compact AVA array with suppressed mutual coupling for 5G mmWave application is proposed in [17]. But, there is still a challenge to reduce the size of AVA arrays and improve their gain.

In this letter, a miniaturized gain-enhanced modified AVA is proposed. Applying gradual corrugated edges (GCEs) and triangular metal directors (MDs) to the AVA, the performance of AVA is improved at lower frequencies and the gain is enhanced at higher frequencies, respectively. As a result, modified AVA achieves high and flat gain in the whole operating frequency band without increasing the circuit size. Furthermore, a compact and high-gain 1×8 E-plane AVA array consisted of designed AVA elements is also designed, fabricated and measured. The designed AVA array has the dimension of $54.4\times28.2\times0.508$ mm^3 and the maximum gain of 12.9 dB. It means that miniaturization and high-gain of AVA array are realized simultaneously in mmWave frequency band.

II. ANTENNA DESIGN AND ANALYSIS

A. SINGLE AVA DESIGN

Fig. 1(a) shows the conventional AVA (CAVA), which has been designed on Rogers RT 5880 substrate with relative dielectric permittivity of 2.2, a loss tangent of 0.0009, and thickness of 0.508 mm. The length (L) and width (W) of the CAVA is 13.5 mm and 6.8 mm. For the CAVA, the exponential curves (y_1 and y_2) are adopted to form both the inner and outer edges of radiation parts that are on the top and bottom surfaces of the substrate. Furthermore, such exponential curve (y_3) is also implemented as a balun to offer more degrees of design freedom to achieve improved impedance matching. The three curves are defined by the following relations:

$$y_1 = c_1 \times \exp(-0.25x) + c_2 (0 \le x \le 8.8 \text{ mm}) \quad (1)$$

$$y_2 = c_3 \times \exp(-1.4x) + c_4 (6.8 \text{ mm} \le x \le 8.8 \text{ mm}) \quad (2)$$

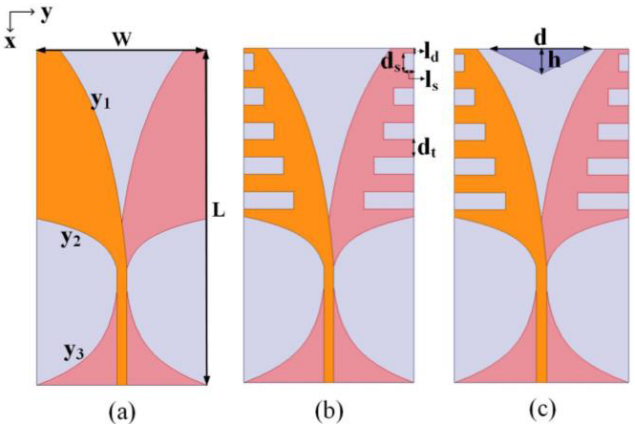

FIGURE 1. Design procedures and geometry of the AVA structures. (a) CAVA. (b) CAVA with GCEs. (c) CAVA with GCEs and MDs.

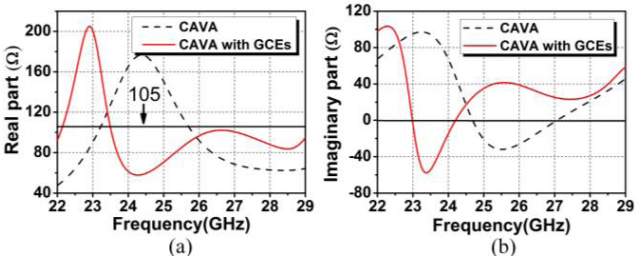

FIGURE 2. Simulated input impedances of the CAVA with and without GCEs. (a) Real part. (b) Imaginary part.

$$y_3 = c_5 \times \exp(0.8x) + c_6 (9.7 \text{ mm} \le x \le 13.5 \text{ mm}) \quad (3)$$

where $c_1 = -3.04$ mm, $c_2 = 3.94$ mm, $c_3 = -4.64 \times 10^4$ mm, $c_4 = 3.41$ mm, $c_5 = -6.86 \times 10^{-5}$ mm, $c_6 = 3.36$ mm. The width of microstrip feedline is fixed on 0.4 mm and the corresponding port impedance is 105-Ω in order to match with power divider at the time of array design. To optimize the antenna performance, a full-wave analysis is carried out and performed by electromagnetic (EM) simulator, *Altair FEKO 7.0*.

However, the CAVA at lower frequencies exhibits low gain performance, which is caused by the unwanted surface currents that radiate vertically with end-fire direction at the outer edge of the radiation arms. So, two methods are introduced to improve the performance of CAVA. One is that the ends of radiation arms are broadened to bring more effective radiation, as shown in Fig. 1(a). On the other hand, gradual corrugated edges (GCEs) are applied to the arms of the CAVA for the gain and miniaturized performance improvement at the low frequencies, shown in Fig. 1(b). The width and length of the first edge are d_s and l_s, and the distance from the top edge of the antenna to the first edge is l_d. The widths of the other edges are kept equal with the first one, but the lengths increase with a common difference l_s gradually. Spacing between two edges is set to d_t.

In Fig. 1(b), from the point of view of impedance matching, GCEs can be seen as some slot-loads to match the

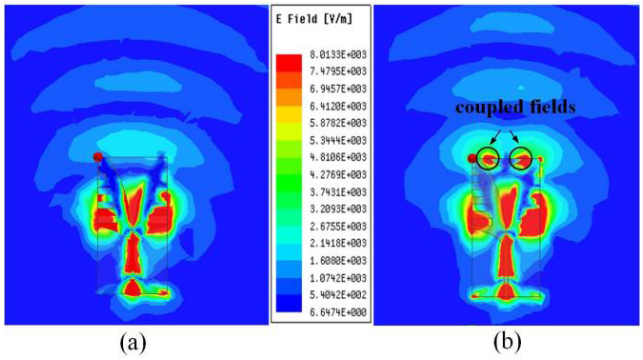

FIGURE 3. Simulated E-field distributions inside the structure at 26 GHz. (a) Without MDs. (b) With MDs.

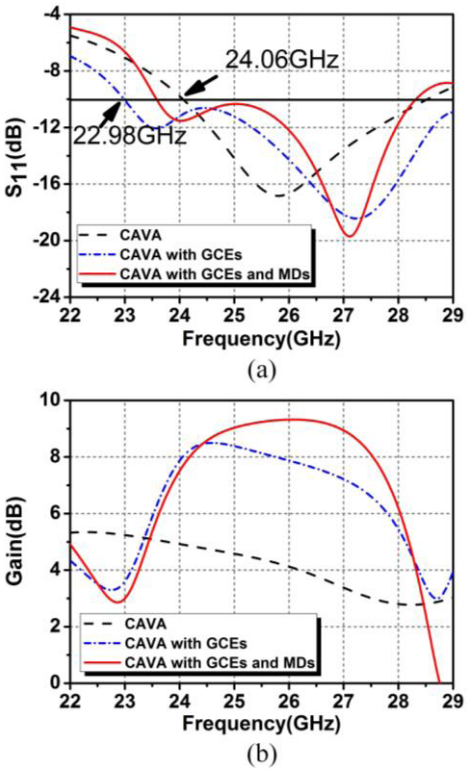

FIGURE 4. Simulated (a) S_{11} and (b) gain variation of the designed antennas.

termination. Loaded slots will change the return loss of the CAVA. This is because the slot-load can be characterized as an RLC resonator and its resonant frequency is related to the size of the slot. The simulated input impedances of the CAVA with and without GCEs are compared in Fig. 2. Results show that the real part of the input impedance of the CAVA with GCEs is closer to 105-Ω but its imaginary part has little improvement. Thus, the impedance matching is significantly improved and a wide bandwidth can be achieved by manipulating the slot length and width. After an extensive simulation on the parameters of corrugated edges, d_s, l_s, l_d and d_t, their optimal values are selected to be 0.7 mm, 0.4 mm, 0.2 mm and 0.7 mm, respectively.

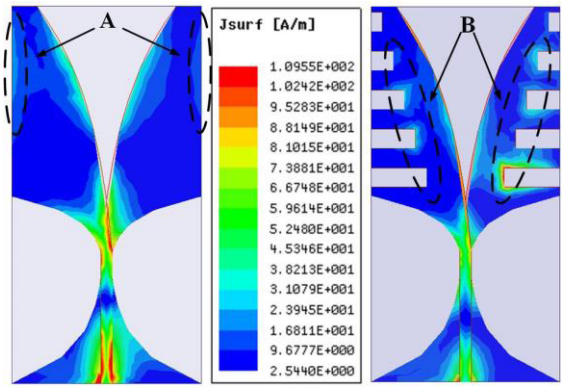

FIGURE 5. Surface current distributions in (a) CAVA, (b) CAVA with GCEs at 22.98GHz.

Furthermore, two triangular metal patches called metal directors (MDs) are added on the two surfaces of the radiation aperture of the CAVA with GCEs in order to improve the gain at higher frequencies. The corresponding model is shown in Fig. 1(c). To explain effectiveness of the MDs on gain improvement, the E-field distributions inside the structure with and without MDs at 26 GHz are given in Fig. 3. Employing MDs with the proposed structure provides a different propagation environment on the antenna aperture. This pair of MDs strengthens the field coupling between two arms of the antenna so that the EM wave that radiates to the space is closer to the plane wave after the superposition of the coupled fields. A parametric study on the various length (d) and height (h) of triangular MDs for gain variation is performed, resulting in that the highest gain is obtained at $d = 4$ mm and $h = 1$ mm (figure not shown for brevity).

The simulated S_{11} of the three antennas are plotted in Fig. 4(a). Results show that the impedance bandwidth of the CAVA is from 24.06 to 28.53 GHz that covers the desired 5G communication band. It is obviously seen that the use of GCEs extends the low end of the frequency band from 24.06 to 22.98 GHz. That is to say, impedance matching performance is improved and miniaturization circuit is realized. There has a slight influence on S_{11} when adding MDs to CAVA with GCEs, as shown in Fig. 4(a).

As shown in Fig. 5, the surface current distribution behaviors of CAVA with and without GCEs at 22.98 GHz are compared. In the region A of Fig. 5(a), it is evident that the surface current density of the CAVA is weak. Comparatively, the excited surface currents in region B of Fig. 5(b) are effectively meandered by adding the GCEs. It leads to a greatly extended current path for a fixed dimension. This behavior results in a lower fundamental resonant frequency and size reduction of a large antenna can be obtained [18].

Gain of the three designed antennas are presented and compared in Fig. 4(b). From the presented results, it is observed that the gain is significantly improved when the GCEs structure is introduced, especially at lower frequencies. Besides, the use of the pair of MDs contributes to the enhancement

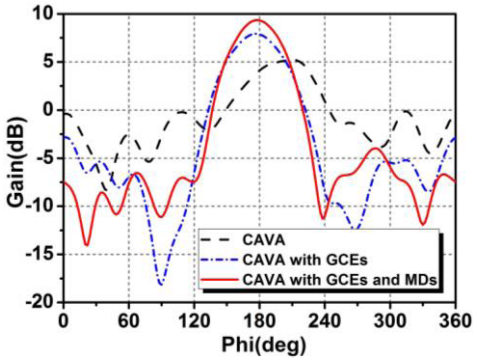

FIGURE 6. Simulated E-plane radiation patterns of three antennas at 26GHz.

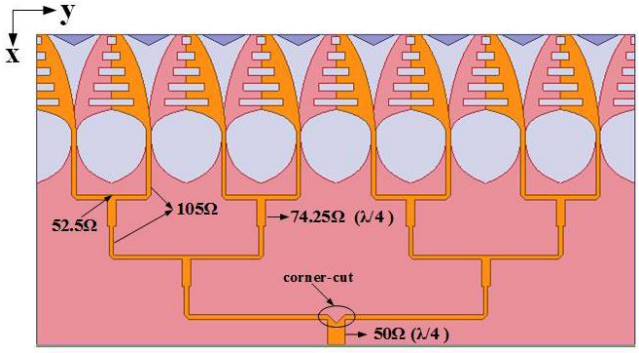

FIGURE 7. Configuration of the proposed AVA array with T-junction power divider.

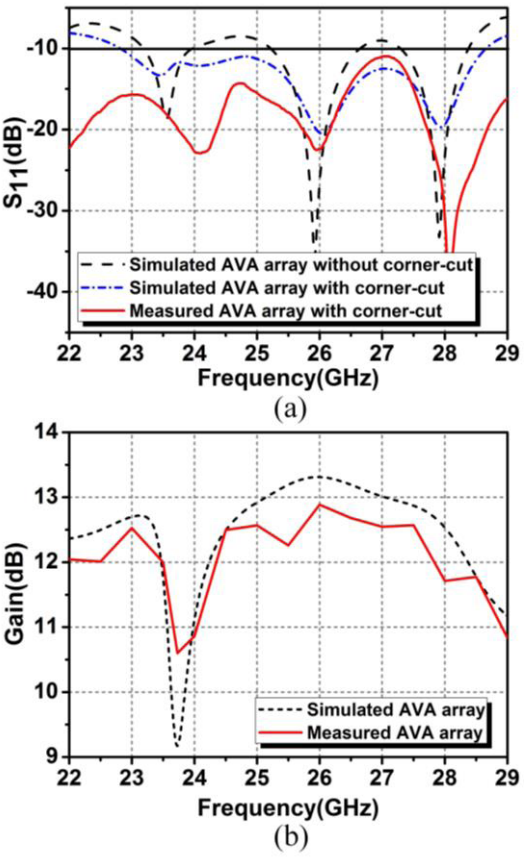

FIGURE 8. (a) Simulated and measured S_{11}. (b) Gain variation of the proposed AVA array.

of gain at higher frequencies. Compared with the CAVA, the gain of the proposed CAVA with GCEs and MDs is further improved with the value more than 5.5 dB and keeps constant within the 5G operating frequency band. It is noted that the maximum gain of the proposed CAVA with GCEs and MDs reaches 9.3 dB at 26 GHz.

In addition, the simulated E-plane (xoy plane) radiation patterns of the three antennas excited at 26 GHz are plotted in Fig. 6. The slight asymmetry of the pattern of CAVA is probably due to some unbalanced mode that reached the antenna from the 'limited length' tapered balun (curve y_3 in Fig. 1(a)), as well as to radiation from the unshielded microstrip line [4]. However, it can be seen that the maximum radiation direction has been fixed in the end-fire direction and the side-lobe level greatly reduces by applying the GCEs. Also, the beamwidth of the main-lobe becomes narrower due to MDs. Therefore, by adding GCEs and MDs, the surface current distribution of antenna has been changed and more surface current distributes along the corrugated edges instead of the edges of the radiate arms. This effect actually produces more directive radiation than the CAVA. Consequently, correcting squint effect, mitigating the side and back lobe levels and increasing its main lobe gain are obtained.

B. ARRAY DESIGN

To achieve higher gain and better directivity, the proposed CAVA with GCEs and MDs is utilized to compose a 1×8 E- plane array. Fig. 7 illustrates the configuration of the proposed AVA array with 1-to-8 T-junction power divider, which can excite each radiating element with equal magnitude. The width of the input port of power divider is set 1.56 mm in order to match 50-Ω coaxial line. Large space between each antenna element may bring grating lobe, but a close distance could cause strong mutual coupling. The element spacing d_a, which is 6.8mm, equals the width of a single element. This spacing is acquired based on a simple grating lobe analysis, as indicated below.

$$d_a < \frac{\lambda_0}{1 + |\cos \varphi_0|} \tag{4}$$

where d_a is the element spacing, λ_0 is the wavelength at the operating frequency, and φ_0 is the main beam angle. For this 8-element AVA array, only the broadside situation (in the E-plane) needs to be considered. In a broadside situation, φ_0 equals 90 degrees, so $d_a < \lambda_0$. The array spacing of 6.8mm is 0.6 times the wavelength at 26GHz in order to prevent grating lobes over the entire frequency band. The characteristic impedances and lengths of power divider are also presented in Fig. 7. The proposed AVA array has a compact size of $4.71\lambda \times 2.44\lambda \times 0.04\ \lambda$ (λ is the wavelength corresponding to 26 GHz).

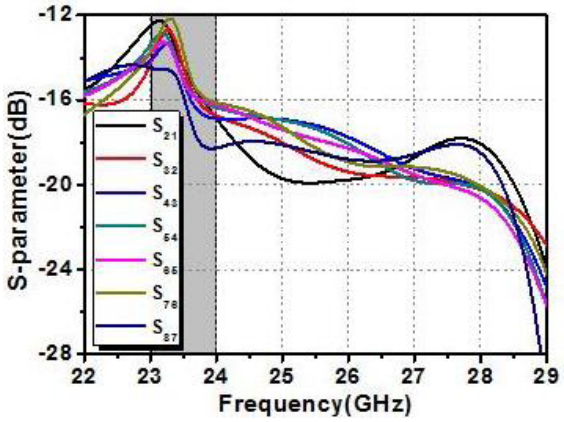

FIGURE 9. Simulated mutual coupling characteristics of AVA array.

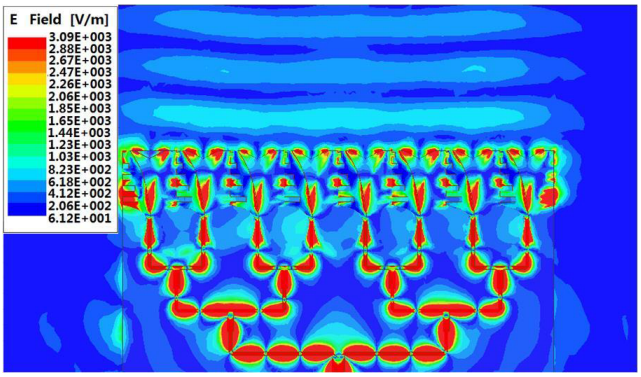

FIGURE 10. Simulated E-field distribution of the proposed AVA array at 26 GHz.

Fig. 8(a) shows the simulated S_{11} of the proposed AVA array. It is noted that corner-cut technique is introduced to the power divider for achieving better impedance matching. As shown in Fig. 8(a), the designed AVA array has a good performance in the frequency range of 22.81 to 28.66 GHz, which contains potential candidate frequency band (24.75-27.5 GHz) of 5G communication. Simulated gain of the proposed AVA array is showed in Fig. 8(b). It is observed that the AVA array presents a gain of 12.75-13.31 dB within the desired 5G frequency band. However, it is seen that the gain drops at 23.7 GHz in Fig. 8(b). This may be caused by the strong mutual coupling between array elements. From simulated S-parameter results of the AVA array (before the power divider is added) in Fig. 9, the mutual coupling is strong in the frequency band of 23-24 GHz and the maximum value can reach −12.5 dB. So, strong coupling causes significant degradation on antenna gain.

To further demonstrate the high gain characteristics, the simulated E-field distribution at 26 GHz of the proposed AVA array is given in Fig. 10. It can be seen that plane-like waves can be obtained. Also, it should be noted that the usage of the microstrip feed network has influence on the gain of

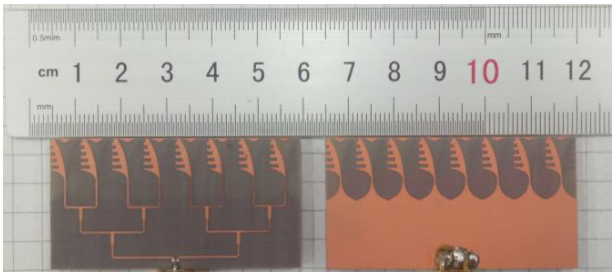

FIGURE 11. Photograph of the fabricated AVA array.

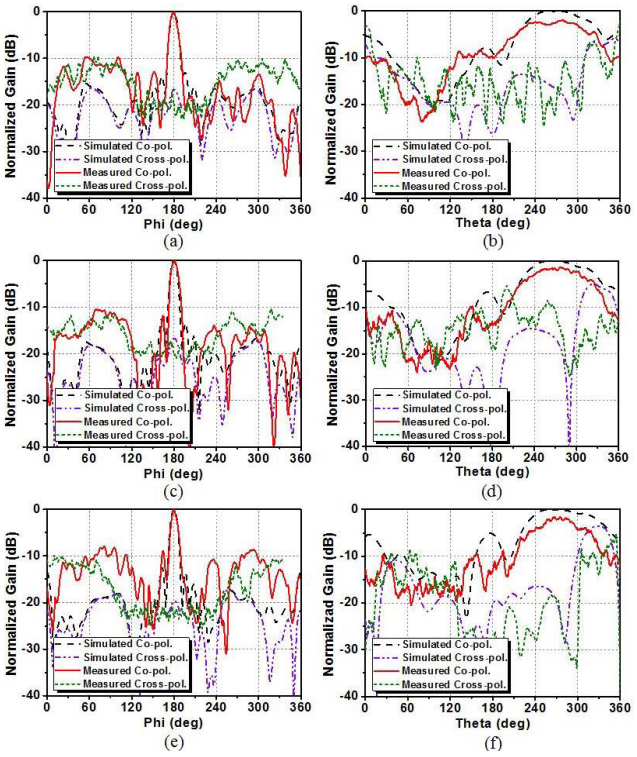

FIGURE 12. Simulated and measured normalized radiation patterns of the proposed AVA array: (a) E-plane at 25 GHz, (b) H-plane at 25 GHz, (c) E-plane at 26 GHz, (d) H-plane at 26 GHz, (e) E-plane at 27 GHz, (f) H-plane at 27 GHz.

proposed AVA array because of the large insertion loss of microstrip line at higher frequencies.

III. MEASURED RESULTS AND DISCUSSION

Following the design procedure, the final AVA array with the power divider has been fabricated and presented in Fig. 11. The measured S_{11} of the AVA array is plotted in Fig. 8(a). As can be observed from the figure, S_{11} of the AVA array is less than −10 dB in the frequency band of 22-29 GHz, which still covers the future 5G communication frequency band. However, the measured S_{11} from 22 GHz to 24.5 GHz fall below −10 dB compared with simulated ones. This phenomenon may be caused by dielectric loss and connector loss. Within the desired frequency band, the measured gain of the AVA array varies in the range of 12.3-12.9 dB, as presented in Fig. 8(b). The performance of devices is sensitive to a

TABLE 1. Comparison of some previous vivaldi antenna array literatures.

Ref.No.	Number of feed	Feed type	Number of element	ε_{eff}	Operating frequency (GHz)	Size ($\lambda \times \lambda \times \lambda$)	Max gain (dB)	
							Simulated	Measured
[16]	1	SIW	8	2.2	38.9-45.1	7.95 × 7.45 × 0.04	16.6	15.9
[19]	1	SIW	8	2.2	26.5-40	6.65 × 3.35 × 0.06	16	N.M
[20]	1	SIW	8	3.38	8-12	4 × 3.6 × 0.32	N.M	16.5
[21]	1	ML	4	3.55	9-12	> 2.99 × 1.36 × 0.02	N.M	6
[22]	1	ML	4	5.7	59-64	6.29 × 5.91 × 0.28	11.57	11.1
[17]	1	ML	8	2.2	24.6-28.5	6.22 × 2.99 × 0.08	11.2	11.32
This work	1	ML	8	2.2	24.75-27.5	4.71 × 2.44 × 0.04	13.31	12.9

SIW represents the substrate integrated waveguide, ML represents the microstrip line, N.M states the not mentioned, and λ is the wavelength at the center frequency of the operating band.

slight change in size, especially in mmWave or sub-mmWave bands. So, there are some discrepancies for measured results that can be due to inaccuracy in fabrication of the antenna and the connector.

Fig. 12 plots the simulated and measured normalized radiation patterns of the AVA array, including co- and cross-polarization in the E- and H-planes at 25 GHz, 26 GHz and 27 GHz, respectively. It can be clearly seen that the half-power beamwidth (HPBW) of the AVA array becomes narrower as the frequency increases. According to the depicted normalized radiation patterns, low cross-polarization levels (about -20dB in the end-fire direction) is achieved. Because the AVA elements are arranged in E-plane, the E-plane radiation pattern has a very narrow main lobe and a low side-lobe level. Moreover, the radiation patterns have good symmetry. In Fig. 12 (b), (d), (f), it is noted that there is a slight mismatch between simulated and measured normalized gain in H-plane, which may be caused by measurement error.

The comparison of proposed AVA array with other various Vivaldi antenna array designs is summarized in Table I. It is seen that [16], [19], and [20] are fed by SIW feed network for its low insertion loss and broadband performance in mmWave range. So, these arrays can achieve high gain but their sizes are large. The gains of [17], [21], and [22] and this work are relatively lower than above-mentioned arrays due to the large insertion loss of microstrip line especially at higher frequencies. Although [21] can realize the small size, the gain is low. Then, [22] has low gain in comparison to this work, and the size is also large. Besides, numerous grounding vias are added to prevent the excitation of cavity modes and reduce electromagnetic leakage, which increase the fabricate difficulty. It is noted that the proposed AVA array outperforms the work in [17] in terms of miniaturization under the similar working frequency band. The size reduction is mainly achieved by GCEs. Also, the gain of the AVA array is found to be competitive when compared with the other designs.

IV. CONCLUSION

In this letter, a miniaturized gain-enhanced AVA with bandwidth from 23.58 to 28.32 GHz is presented. Low end of frequency band has been extended and gain at lower frequencies has been improved by GCEs at each radiate arm. Two triangular MDs are added to improve the gain at higher frequencies without the need of extra circuit size. Then, a low-profile and high-gain AVA array in combination with a 1-to-8 T-junction power divider is designed, fabricated and measured. The array is operating in the band of 24.75-27.5 GHz, which is ideal for 5G communication. Furthermore, the array has a maximum gain of 12.9 dB, symmetrical radiation patterns and compact structure, which makes it a good candidate for integration in devices for 5G communication applications.

ACKNOWLEDGMENT

The authors would like to thank the Associate Editor and the reviewers for their useful comments.

REFERENCES

[1] P. Gupta, "Evolvement of mobile generations: 1G to 5G," *Int. J. Technol. Res. Eng.*, vol. 1, pp. 152–157, 2013.
[2] K. S. Yngvesson, T. L. Korzeniowski, Y.-S. Kim, E. L. Kollberg, and J. F. Johansson, "The tapered slot antenna-a new integrated element for millimeter-wave applications," *IEEE Trans. Microw. Theory Techn.*, vol. 37, no. 2, pp. 365–374, Feb. 1989.
[3] P. J. Gibson, "The Vivaldi aerial," in *Proc. 9th Eur. Microw. Conf.*, Brighton, U.K., Oct. 1979, pp. 101–105.
[4] E. Gazit, "Improved design of the Vivaldi antenna," *IEE Proc. H Microw., Antennas Propag.*, vol. 135, no. 2, pp. 89–92, Apr. 1988.
[5] M. Moosazadeh, S. Kharkovsky, J. T. Case, and B. Samali, "Antipodal Vivaldi antenna with improved radiation characteristics for civil engineering applications," *IET Microw., Antennas Propag.*, vol. 11, no. 6, pp. 796–803, May 2016.
[6] S.-A. Malakooti, M. Moosazadeh, D. C. Ranasinghe, and C. Fumeaux, "Antipodal Vivaldi antenna for sum and difference radiation patterns with reduced grating lobes," *IEEE Antennas Wirel. Propag. Lett.*, vol. 1, pp. 3139–3142, 2017.
[7] A. M. D. Oliveira, M. B. Perotoni, S. T. Kofuji, and J. F. Justo, "A palm tree antipodal Vivaldi antenna with exponential slot edge for improved radiation pattern," *IEEE Antennas Wireless Propag. Lett.*, vol. 14, pp. 1334–1337, 2015.
[8] Z. Briqech, J. Robitaille, K. Bishyk, K. Abdo, D. Bhogal, and A. Sebak, "High gain antipodal tapered slot antenna With sine-shaped corrugation and Fermi profile substrate slotted cut-out for MMW 5G," in *Proc. Global Symp. Millim.-Waves (GSMM)*, May 2015, pp. 1–3.
[9] M. Moosazadeh, S. Kharkovsky, J. T. Case, and B. Samali, "Improved radiation characteristics of small antipodal Vivaldi antenna for microwave and millimeter-wave imaging applications," *IEEE Antennas Wirel. Propag. Lett.*, vol. 1, pp. 1961–1964, 2017.

[10] M. Moosazadeh and S. Kharkovsky, "A compact high-gain and front-to-back ratio elliptically tapered antipodal Vivaldi antenna with trapezoid-shaped dielectric lens," *IEEE Antennas Wireless Propag. Lett.*, vol. 15, pp. 552–555, 2016.
[11] I. T. Nassar and T. M. Weller, "A novel method for improving antipodal Vivaldi antenna performance," *IEEE Trans. Antenna Propag.*, vol. 63, no. 7, pp. 3321–3324, Jul. 2015.
[12] M. Amiri, F. Tofigh, A. Ghafoorzadeh-Yazdi, and M. Abolhasan, "Exponential antipodal Vivaldi antenna with exponential dielectric lens," *IEEE Antennas Wireless Propag. Lett.*, vol. 1, pp. 1792–1795, 2017.
[13] B. Zhou and T. J. Cui, "Directivity enhancement to Vivaldi antennas using compactly anisotropic zero-index metamaterials," *IEEE Antennas Wireless Propag. Lett.*, vol. 10, no. 4, pp. 326–329, 2011.
[14] X. Li, H. Zhou, Z. Gao, H. Wang, and G. Lv, "Metamaterial slabs covered UWB antipodal Vivaldi antenna," *IEEE Antennas Wireless Propag. Lett.*, vol. 16, pp. 2943–2946, 2017.
[15] N. O. Parchin, M. Shen, and G. F. Pedersen, "Small-size tapered slot antenna (TSA) design for use in 5G phased array applications," *Appl. Comput. Electromagn. Soc. J.*, vol. 32, no. 3, pp. 193–202, 2017.
[16] P. Liu, X. Zhu, X. Wang, and L. Tian, "A SIW-based Vivaldi array antenna for 5G wireless communication systems," in *Proc. IEEE Int. Symp. Antennas Propag. USNC/URSI Nat. Radio Sci. Meeting*, Jul. 2017, pp. 529–530.
[17] S. Zhu, H. Liu, P. Wen, and Z. Chen, "A compact gain-enhanced Vivaldi antenna array with suppressed mutual coupling for 5G mmWave application," *IEEE Antennas Wireless Propag. Lett.*, vol. 17, no. 5, pp. 776–779, May 2018.
[18] K. L. Wong, *Compact and Broadband Microstrip Antennas*. Hoboken, NJ, USA: Wiley, 2002.
[19] J. Puskely and T. Mikulášek, "Compact wideband Vivaldi antenna array for microwave imaging applications," in *Proc. IEEE Eur. Conf. Antennas Propag.*, Apr. 2013, pp. 1519–1522.
[20] R. Kazemi, A. E. Fathy, and R. A. Sadeghzadeh, "Dielectric rod antenna array with substrate integrated waveguide planar feed network for wideband applications," *IEEE Trans. Antennas Propag.*, vol. 60, no. 3, pp. 1312–1319, Mar. 2012.
[21] R. Sturdivant and E. K. P. Chong, "Dielectric notch radiator antennas with integrated filtering for 5G and IoT access," in *Proc. IEEE Radio Wireless Symp. (RWS)*, Jan. 2017, pp. 197–200.
[22] G. Brzezina, R. E. Amaya, A. Petosa, and L. Roy, "Broadband and compact Vivaldi arrays in LTCC for 60 GHz point-to-point networks," in *Proc. Wireless. Microw. Technol. Conf.*, Jun. 2014, pp. 1–5.

HAIWEN LIU received the B.S. degree in electronic system and the M.S. degree in radio physics from Wuhan University, Wuhan, China, in 1997 and 2000, respectively, and the Ph.D. degree in microwave engineering from Shanghai Jiao Tong University, Shanghai, China, in 2004. From 2007 to 2008, he was a Professor with the Institute of Optics and Electronics, Chengdu, China, where he was supported by the 100 Talents Program of the Chinese Academy of Sciences. Since 2009, he has been a Chair Professor with East China Jiaotong University, Nanchang, China. He is currently a Full Professor with Xi'an Jiaotong University, Xi'an, China. He has published over 100 papers in international and domestic journals and conferences. His current research interests include the electromagnetic modeling of high-temperature superconducting circuits, radio frequency and microwave passive circuits and systems, antennas theory, and radar systems.

WENJUAN YANG was born in Gansu, China, in 1994. She received the B.S. degree in communication engineering from Xi'an Jiaotong University, Xi'an, China, in 2016, where she is currently pursuing the M.S. degree with the School of Electronic and Information Engineering. Her current research interests include ultra-wide-band antenna theory and design, antenna array, and filtering antenna.

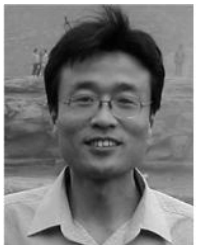

ANXUE ZHANG received the B.S. degree in electrical engineering from Henan Normal University, Xinxiang, China, in 1996, and the M.S. and Ph.D. degrees in electromagnetic and microwave engineering from Xi'an Jiaotong University, Xi'an, China, in 1999 and 2003, respectively. He was a Visiting Scientist with Auburn University, Auburn, AL, USA, from 2008 to 2009. He is currently an Associate Professor with Xi'an Jiaotong University. His main research fields include antenna and electromagnetic wave propagation, RF and microwave circuit design, ultra-wide-band technology, and left-hand materials applications.

SHUANGSHUANG ZHU was born in Henan, China, in 1991. She received the B.S. degree in electronic engineering from the North China University of Water Resources and Electric Power, Zhengzhou, China, in 2012, and the M.S. degree in communication and information system from East China Jiaotong University, Nanchang, China, in 2015. She is currently pursuing the Ph.D. degree with the School of Electronic and Information Engineering, Xi'an Jiaotong University, Xi'an, China. Her current research interests include antenna array, millimeter-wave antenna, and metasurface.

ZHENGBIAO WANG (S'17) received the B.S. degree in communication engineering information system from East China Jiaotong University, Nanchang, China, in 2017, where he is currently pursuing the M.S. degree in communication engineering information system. His current research interests include antenna theory and design, and spoof surface plasmon polaritons.

TAOTAO HUANG received the B.S. degree in automation engineering and the M.S. degree in electromagnetic field and microwave technology from the Xi'an University of Posts and Telecommunications, Xi'an, China, in 2014 and 2017, respectively. He is currently pursuing the Ph.D. degree with Xi'an Jiaotong University, Xi'an. His research interests include microstrip antenna and dielectric resonator antenna.